Original Article

Impact of Chemical Reaction on Methanol-Silica-Titania Hybrid Nanofluid Filled Couette Channel

Khasim Ali[1], Y. Rajashekhar Reddy[2], Balla Chandra Shekar[3]

[1]Department of Mathematics, Nawab Shah Alam Khan College of Engineering and Technology, Hyderabad, Telangana, 500024, India.

[2]Department of Mathematics, Jawaharlal Nehru Technological University Hyderabad, College of Engineering Jagtial, Telangana, 505501, India.

[3]Department of Mathematics, Sreenidhi University, Yamnapet, Hyderabad, Telangana, 501301, India.

Email: kasimalishaik@gmail.com

DOI: 10.47750/pnr.2022.13.S09.226

Abstract

Current paper focusses on the numerical simulation of two phase nanofluid flow in Couette channel containing novel SiO2-TiO2-CH3OH hybrid nanofluid (HNF). The hybrid nanoparticles silica(SiO2) and titania(TiO2) are added to base fluid methanol(CH3OH) in 1:1 ratio. The lower wall of channel is fixed, while the upper is set in uniform motion with convective cooling. The governed non-linear partial differential expressions(PDE) are answered employing finite difference method (FDM). A comparison of effect of hybrid nanofluid versus nanofluid (NF) is performed. The upshots of dimensionless quantities namely. nanoparticle volume fraction, magnetic field, chemical reaction parameter, Brownian motion and thermophoresis and Eckert number are reported graphically. The results demonstrate that SiO2-TiO2-CH3OH HNF shows significant impact over SiO2-CH3OH NF on velocity, temperature and concentration in the Couette channel.

Keywords: Couette flow, hybrid nanofluid, Brownian motion, thermophoresis, magnetic field, two phase nanofluid model, chemical reaction parameter.

1. INTRODUCTION

Suspension of nanometer-sized particles has been witnessed higher thermal conductivity. This homogeneous non-crystalline substance of nanoparticles(NPs) in to base liquid has been renowned as 'nanofluid(NF)' by Choi and Eastman [1,2]. Today, the NFs have revealed a hopeful impending as thermal liquids for several heat transfer(HT) applications[3], in solar thermal collection [4,5], to improve the HT coefficient. Substantial volume of research [6-8] is taken place on the nanofluid flow problems using Tiwari and Das's model[6], known as single-phase nanofluid model. Saha and Paul [9] explored turbulance flow of H2O-based alumina and titania NFs in a pipe under persistent heat flux boundary condition via singlephase(homogeneous) approach and thermo-dependent characteristics. Manca et al. [10] examined NF convection of Al2O3/H2O in 2-D channel with uniform heat flux by means of single-phase(homogeneous) model and the properties were supposed thermo-independent. Ahmed et al. [11] investigated convection HT from pipe with fixed wall thermos restrictions. Vajjha et al. [12] examined HT presentation of C2H6O2/H2O-based Al2O3 and CuO NFs in horizontal conduit of a radiator.

The two-phase model suggested by Buongiorno [13], in which nanoparticle concentration is assumed to be inhomogeneous. This model is frequently applied in literature [14-18] for its simplicity and accuracy. Mahmoodi and Kandelousi [14], for instance, considered kerosene– Al2O3 NF flow between two parallel plates based on Buongiorno [13] model to account for the particle migration effects on heat transfer coefficients. They reported that Brownian motion and thermophoresis enhance the temperature profile. Ali and Makinde [19] examined the Buongiorno's approach of NF to analyze transient generalized Couette flow of NFs. Tlili et al. [20] reported water based NF CouettePoiseuille flow in conduit. Cylinderical Couette flow of copper-H2O NF utilizing single/two phase model is examined by Hajmohammadi [21]. Karim et al. [22] examined the influence of variate viscosity on Cu-H2O NF flow past Couette conduit of fixed lower plate.

Hybrid nanofluid (HNF) is formed by combining two or more types of NPs in the suspension of base liquid and useful in all areas of HT like manufacturing, electro-sensor and thermal biosensors, and acoustic wave sensors [23-25]. Hayat and Nadeem [26] reported influence of HT of silver–copper oxide/water HNF. Ghadikolaei et al. [27] investigated the aspect of NPs to study the behavior of TiO2– copper oxide /ethyleneglycol–water HNF over revolving cone. Waini et al. [28] explored the HNF flow

past a nonlinear porous shrink/enlarge wall. Bagheri et al. [29] performed sensitive-analysis of HNF considering heat flux. The upshots of viscous dissipation on Cu–Al2O3–H2O HNF past shrinking plate are investigated by Lund et al. [30]. Swain et al. [31] investigated influence of chemical reaction of MWCNT/Iron oxide– water HNF past an exponential shrink permeable plate with slip boundary conditions(BCs). They concluded that Schmidt number and chemical reaction boost mass transfer(MT) rate. Sheikholeslami et al. [32] explored HT and MT aspects of transient NF flow in between parallel plates. The significant result of Brownian motion and thermophoresis have been considered in the approach of nanofluid. Ghalambaz et al. [33] inspected the HNF flow in four sided cavity. Xuan et al. [34] scrutinized the impact of surface plasmon resonance of TiO2-Ag-H2O NPs for photo thermal performance. Madhesh et al. [35] analyzed coppertitania/water HNF, while Sundar et al. [36] analyzed an MWCNT–Fe3O4/water hybrid nanofluid. An exceptional analysis of applied advances of HNFs can be noticed in the effort of Sarkar et al. [37].

Chen and Arce [38] illustrated diffusion convective MT with chemical reaction in Couette flow. Abbaszadeh et al. [39] and Kareem and Gbadeyan [40] investigated the same flow but with exothermic chemical reaction of two step. Ahmad and Kalita [41] focussed on chemicaly reacting fluid over infinite vertical surface. Muthucumaraswamy and Ganesan [42] scrutinized impact of chemically reactive/ injective flow aspects of an isothermal plate and determined that the velocity profile declines with growing chemical reaction. Dulal and Babulal [43] scrutinized collective impacts of viscous dissipative, chemically reactive and Joule heating on transient magnetohydrodynamic(MHD) mixed convection past vertical sheet in permeable medium. The consequences of chemically reactive polar/Newtonian nanofluid flow is studied by several authors[44-46].

The objective of the present article is to examine the 2-dimensional transient Couette flow in using two phase nanofluid model a channel associated with chemical reaction. The channel is supposed to contain HNF methanol-Silica-Titania. To best of authors knowledge, Couette channel flow of hybrid nanofluid methanol-Silica-Titania has not been studied under the influence of chemical reaction. The administered expressions are answered by utilizing FDM and upshots are visualized as 2-Dcontours of flow, and heat and volume fraction distributions. Furthermore, it can be mentioned that a strong correlation of Nusselt number and skin friction is observed with previous findings.

2. Mathematical Formulation

A Couette flow containing hybrid nanoparticles SiO2-TiO2- in the base fluid CH3OH with the impact of chemical reaction. As presented in figure 1, x-axis is assumed alongside plate and y-axis is assumed perpendicularly. Convective condition is considered at top plate (y = h). The governing equations, based on nanofluid models of Tiwari and Das [6] and Buongiorno [13] are:

$$\frac{\partial u}{\partial x} = 0 \qquad (1)$$

$$\rho_{hnf}\frac{\partial u}{\partial \bar{t}} = -\frac{\partial p}{\partial x} + \mu_{hnf}\frac{\partial^2 u}{\partial y^2} - \sigma B_0^2 u \qquad (2)$$

$$\frac{\partial T}{\partial \bar{t}} = \alpha_{hnf}\frac{\partial^2 T}{\partial y^2} + \frac{\mu_{hnf}\,\alpha_{hnf}}{k_{hnf}}\left(\frac{\partial u}{\partial y}\right)^2 + \tau\left[D_B\left(\frac{\partial T}{\partial y}\,\frac{\partial C}{\partial y}\right) + \frac{D_T}{T_a}\left(\frac{\partial T}{\partial y}\right)^2\right]$$

$$\frac{\partial C}{\partial \bar{t}} = D_B\frac{\partial^2 C}{\partial y^2} + \frac{D_T}{T_a}\,\frac{\partial^2 T}{\partial y^2} - K^*(C - C_a) \qquad (3)$$

The constraints at boundary are as follows

$$u = 0,\ T = T_0,\ \ C = C_0 \qquad \text{at} \quad y = 0$$

$$u = U_h,\quad -k_{hnf}\frac{\partial T}{\partial y} = h_f(T - T_\infty),\ D_B\,\frac{\partial C}{\partial y} = -\frac{D_T}{T_\infty}\frac{\partial T}{\partial y} \qquad \text{at} \quad y = h$$

Thermophysical aspects of NF and HNF are given as,

$$\mu_{nf} = \frac{\mu_f}{(1-\phi)^{2.5}}$$

$$\rho_{nf} = (1-\phi)\rho_f + \phi\rho_s$$

$$\alpha_{nf} = \frac{\kappa_{nf}}{(\rho C_P)_{nf}}$$

$$(\rho C_P)_{nf} = (1-\phi)(\rho C_P)_f + \phi(\rho C_P)_s$$

$$\frac{\kappa_{nf}}{\kappa_f} = \frac{(\kappa_{s1}+2\kappa_f) - 2\phi_1(\kappa_f - \kappa_{s1})}{(\kappa_{s1}+2\kappa_f) + \phi_1(\kappa_f - \kappa_{s1})}$$

$$\rho_{hnf} = \left\{(1-\phi_2)\left((1-\phi_1) + \phi_1\frac{\rho_{s1}}{\rho_f}\right) + \phi_2\frac{\rho_{s2}}{\rho_f}\right\}\rho_f$$

$$(\rho C_p)_{hnf} = \left\{(1-\phi_2)\left((1-\phi_1) + \phi_1\frac{(\rho C_p)_{s1}}{(\rho C_p)_f}\right) + \phi_2\frac{(\rho C_p)_{s2}}{(\rho C_p)_f}\right\}(\rho C_p)_f$$

$$\mu_{hnf} = \frac{\mu_f}{(1-\phi_1)^{2.5}(1-\phi_2)^{2.5}}$$

$$\kappa_{hnf} = \frac{(\kappa_{s2}+2\kappa_f) - 2\phi_2(\kappa_f - \kappa_{s2})}{(\kappa_{s2}+2\kappa_f) + \phi_2(\kappa_f - \kappa_{s2})}\kappa_{nf}$$

Table 1: Thermophysical values of methanol, silica and titania.

Physical Properties	**SiO_2**	**TiO_2**	**CH_3OH**
$C_p\ (J/KgK)$	703	686.2	2545
$\rho\ (Kg/m^3)$	2200	4250	792
$k\ (W/mK)$	1.38	8.953	0.2035

The succeeding non-dimensional variable quantity are raised to transform governing expressions into dimensionless form.

-

$$X = \frac{x}{h}, Y = \frac{y}{h},$$

$$U = \frac{u}{U_h} = \frac{hu}{\nu_f}, t = \frac{\tau\nu_f}{h^2} = \frac{\tau U_h}{h}, \quad \theta = \frac{T-T_0}{T_\infty - T_0}, \phi = \frac{C-C_0}{C_\infty - C_0},$$

$$\alpha_f = \frac{k_f}{(\rho C_P)_f}, \bar{P} = \frac{Ph^2}{\rho_f \nu_f{}^2}, \quad Ec = \frac{\nu_f{}^2}{C_P(T_\infty - T_0)h^2}, A = -\frac{\partial \bar{P}}{\partial X}, \quad M = \frac{\sigma B_0^2 h^2}{\mu_f}, Bi = \frac{hh_f}{k_f}$$

$$Pr = \frac{\nu_f}{\alpha_f}, Kr = \frac{K^* h^2}{\nu_f}, \quad Nb = \frac{\tau D_B(C_\infty - C_0)}{\alpha_f}, Nt = \frac{\tau D_T(T_\infty - T_0)}{T_\infty \alpha_f}, Le = \frac{\nu_f}{D_B}$$

The non-dimensional transformed expressions can be simplified as:

$$\frac{\partial U}{\partial t} = \frac{\rho_f}{\rho_{hnf}} \left\{ A + \frac{\mu_{hnf}}{\mu_f} \frac{\partial^2 U}{\partial Y^2} - MU \right\} \quad (8)$$

Temperature equation:

$$\frac{\partial \theta}{\partial t} = \frac{(\rho C_p)_f}{(\rho C_p)_{hnf}} \left\{ \frac{1}{Pr} \frac{k_{hnf}}{k_f} \frac{\partial^2 \theta}{\partial Y^2} + \frac{\mu_{hnf}}{\mu_f} Ec \left(\frac{\partial U}{\partial Y} \right)^2 \right\} + \frac{Nb}{Pr} \frac{\partial \theta}{\partial Y} \frac{\partial \phi}{\partial Y} + \frac{Nt}{Pr} \left(\frac{\partial \theta}{\partial Y} \right)^2$$

$$\frac{\partial \phi}{\partial t} = \frac{1}{Le} \left(\frac{\partial^2 \phi}{\partial Y^2} + \frac{Nt}{Nb} \frac{\partial^2 \theta}{\partial Y^2} \right) - Kr\, \phi \qquad (9) \quad (9)$$

Constraints at the boundary are as follows

$$\text{When } t > 0, \; U = 0, \; \theta = 0, \; \phi = 1 \quad \text{at} \quad Y = 0$$

$$U = 1, \; \frac{\partial \theta}{\partial Y} = -Bi(\theta - 1), \; \frac{\partial \phi}{\partial Y} = -\frac{Nt}{Nb} \frac{\partial \theta}{\partial Y} \quad \text{at} \quad Y = 1 \quad (10)$$

The coefficients skin friction and Nusselt number at bottom, top plates are shown by

$$C_f = \frac{1}{(1-\phi_1)^{2.5}(1-\phi_2)^{2.5}} \frac{\partial U}{\partial Y}_{Y=0,1} \text{ and } \quad Nu = -\frac{k_{hnf}}{k_f} \frac{\partial \theta}{\partial Y}_{Y=0,1}$$

3. Solution scheme

The nonlinear differential equations (8-10) are solved numerically using FDM [19,22]. The first order derivatives are approximated by forward differences and second order derivatives by central differences. The norm of convergence is established when $|\varphi^{n+1} - \varphi^n| \leq 10^{-5}$, where n is number of times repeted and φ designates $[U, \theta, \phi]$. Table 2 shows a comparison of present results to previous studies for special case $\phi = 0$, and an excellent agreement is

Table 2: Comparision of Skin friction and Nusselt number for $\phi = 0$

β	Bi	Skin friction			Nusselt Number		
		Ali and Makinde [19]	Karim et al. [22]	Present Results	Ali and Makinde [19]	Karim et al. [22]	Present Results
0.1	1	0.397	0.395	0.3962	0.512	0.511	0.5121
0.1	3	0.406	0.405	0.4058	0.790	0.784	0.7883
0.5	1	0.145	0.146	0.1443	0.223	0.221	0.2227

4. Discussion

This section is devoted to discuss the computational outcomes of Couette flow of NF encompassing silica (SiO2), titania (TiO2) as nanoparticles and methanol (CH3OH) as base liquid, are established in terms of contours plots and trend lines of velocity and temperature. Figures 1 – 7 discover the profiles of velocity, temperature and nanoparticle concentration of unsteady Couette flow, for the parameters: magnetic field parameter (M=1 – 10), nanoparticle volume fraction(NVF) (=0.01 – 0.25), Biot number (Bi=1), Eckert number (Ec=0.1 – 1), Brownian motion parameter (Nb=0.01 – 0.2), thermophoresis parameter (Nt=0.01

– 0.5) and chemical reaction parameter (Kr=0.1 – 1). Further, figures 8-9 represent the contours of velocity, temperature and concentration, for the variation of time, nanoparticles and NF, HNF. Table 3 displays skin friction for the variation of time parameter, NVF and magneticfield. Table 4 displays Nusselt number for the variation of effective parameters.

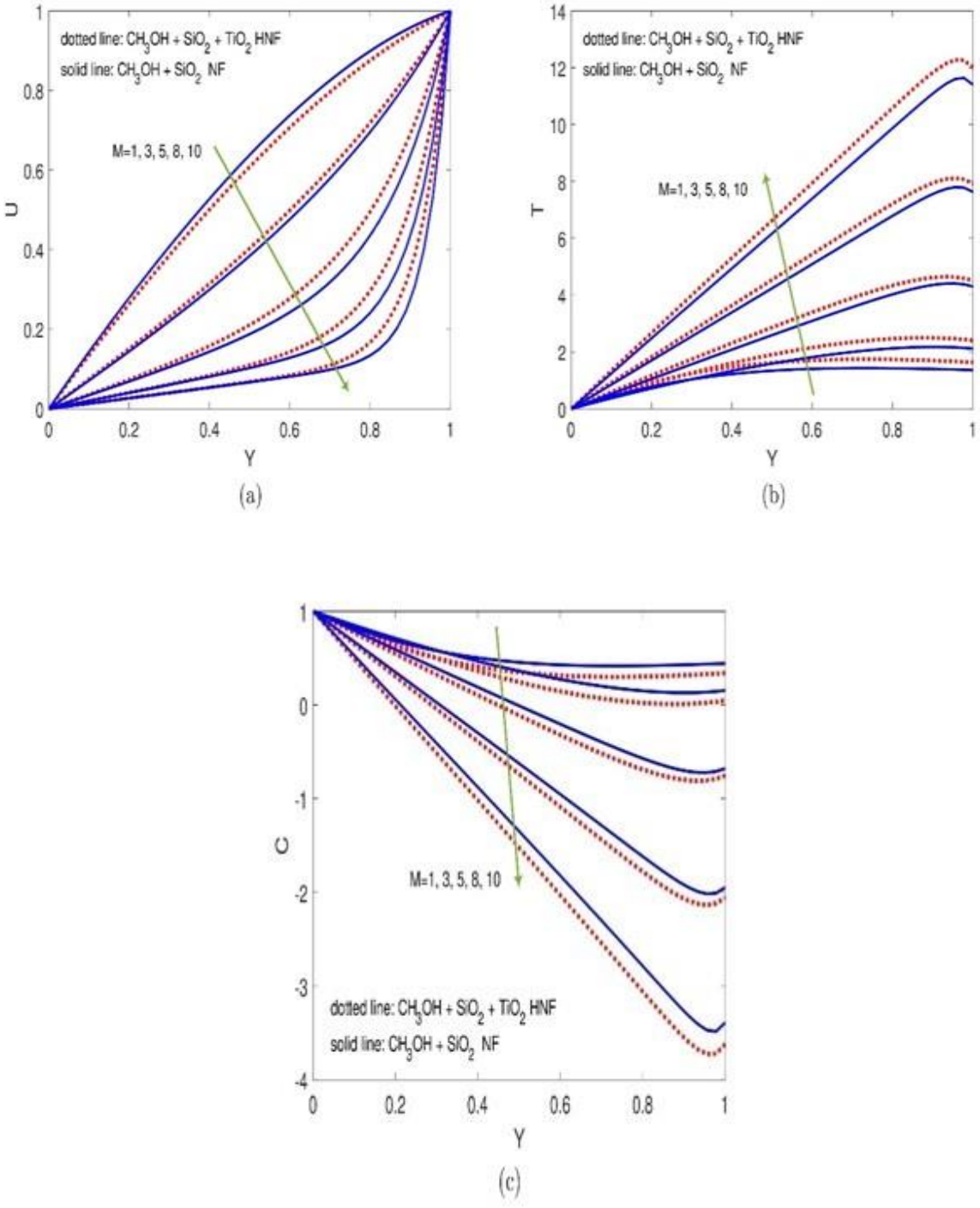

Figure 2: Impression of M on (a) velocity (b) temperature (c) concentration for , Kr=0.1, Ec=1, Pr=6.83, Bi=1, Nb=0.4, Nt=0.16, Le=1.

Figure 2 depicts the impact of magnetic-field on velocity, temperature and concentration for M= 1, 3, 5, 8, 10. From the figure it is detected that an upsurge in magnetic field deteriorates velocity. As the magnetic field rises, Lorenz force produces. This force opposes the motion, so the velocity trend decelerated. The temperature is boosted in channel when the magneticfield

intensified. The nanoparticle concentration shows declining trend with a rise in magneticfield. It is also revealed from the figure that, the nature of boosting/declining resulted by the submission of magnetic-field is dominant in case of SiO2-TiO2-CH3OH HNF than that of SiO2 -CH3OH NF.

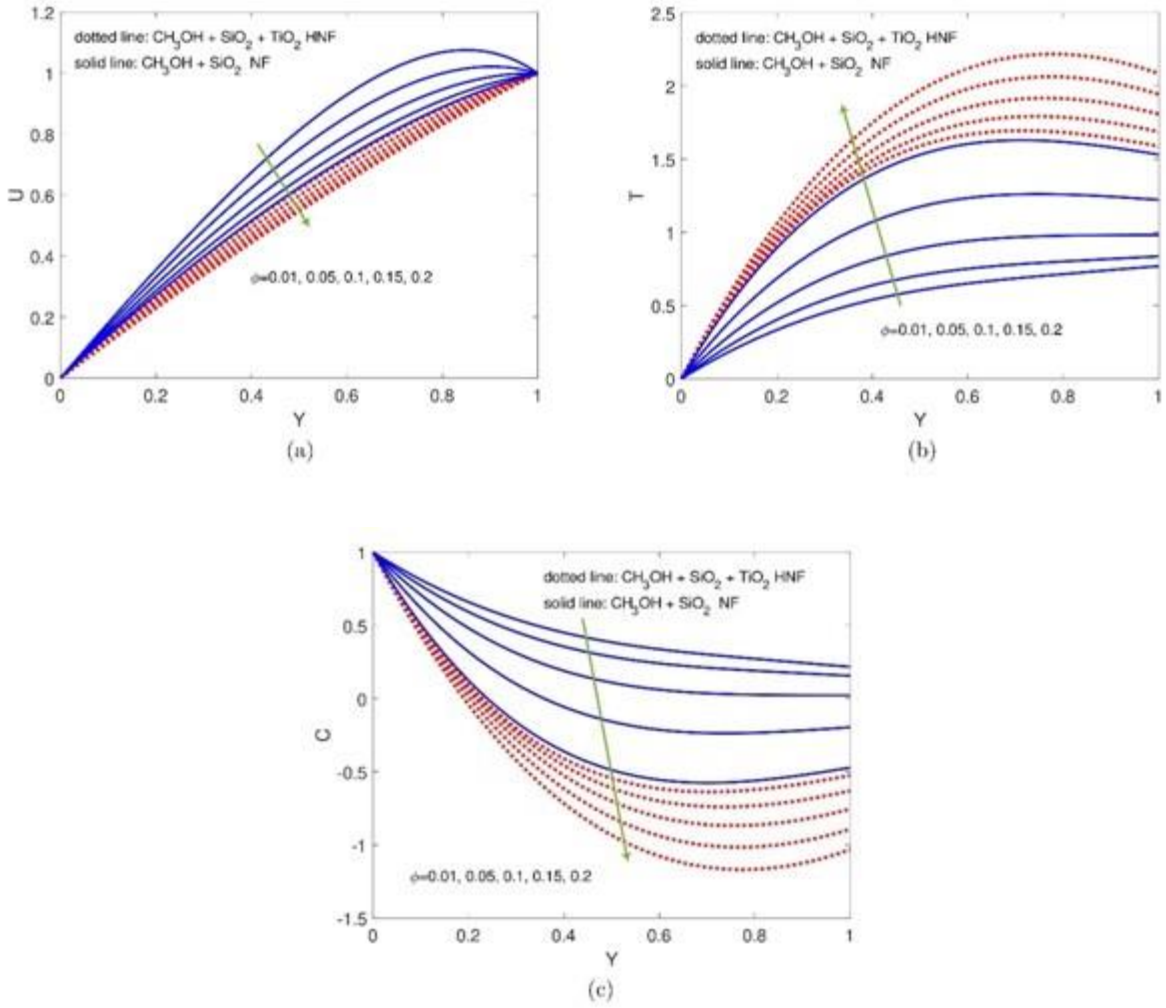

Figure 3: Impression of on (a) velocity (b) temperature (c) concentration for M=1, Kr=0.1, Ec=1, Pr=6.83, Bi=1, Nb=0.4, Nt=0.16, Le=1.

Figure 3 depicts the profiles of velocity, temperature and NP concentration for the disparity of NVF. The upsurge in the NVF deteriorates velocity and concentration in the channel. In contrast, the upsurge in the nanoparticle fraction elevates the temperature in the channel. It is also revealed from the figure that, the nature of boosting/declining resulted by the increment of nanoparticle volume fraction is dominant in case of SiO2-TiO2-CH3OH HNF than that of SiO2 -CH3OH NF. When the volume fraction increases, the thermal conductivity of the NF surges. Thus, upsurge in temperature is noted. The elevation in the temperature is more in case of HNF as the addition of NPs TiO2 improves the thermal conductivity.

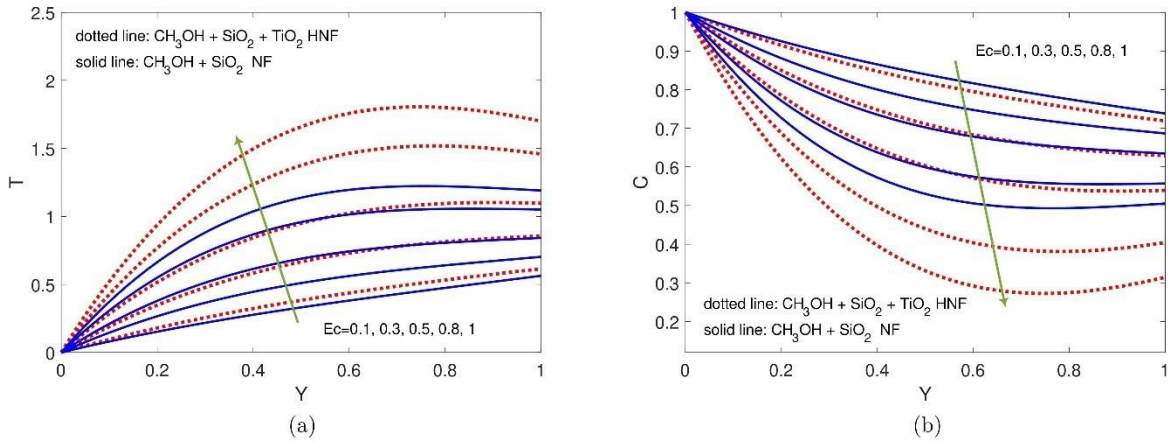

Figure 4: Impression of Ec on (a) velocity (b) temperature (c) concentration for =0.05, M=1, Kr=0.1, Pr=6.83, Bi=1, Nb=0.4, Nt=0.16, Le=1.

Figure 4 portrays the profiles of temperature and NP concentration for the variation of Eckert number(Ec). The upsurge in Ec elevates the temperature and deteriorates the concentration. When Ec increases, the ratio of advective transport to heat dissipation increases. This is the reason for the growth in the temperature profile. It is also revealed from the figure that, the nature of boosting/declining resulted by the increment of Eckert number is dominant in case of SiO2-TiO2-CH3OH HNF than that of SiO2 -CH3OH NF.

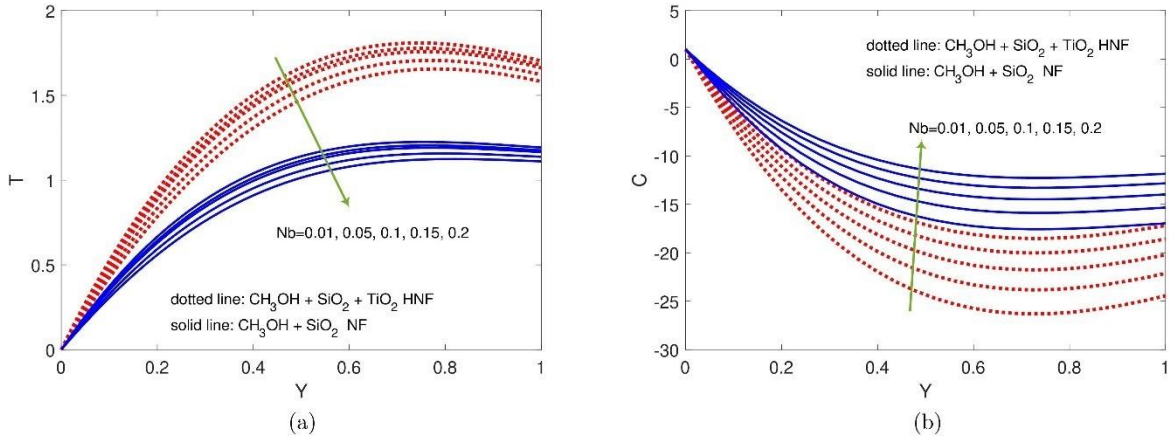

Figure 5: Impression of Nb on (a) velocity (b) temperature (c) concentration for =0.05, M=1, Kr=0.1, Ec=1, Pr=6.83, Bi=1, Nt=0.16, Le=1.

Figure 5 depicts the profiles of temperature and nanoparticle concentration for the variation of Brownian motion. The upsurge in the Brownian motion elevates the concentration in the channel. The temperature in the channel decreases with Brownian motion. The temperature profile is observed to be higher for SiO2-TiO2-CH3OH HNF than that of SiO2 -CH3OH NF. The concentration profile is observed to be lower for of SiO2-TiO2-CH3OH HNF than that of SiO2 -CH3OH NF.

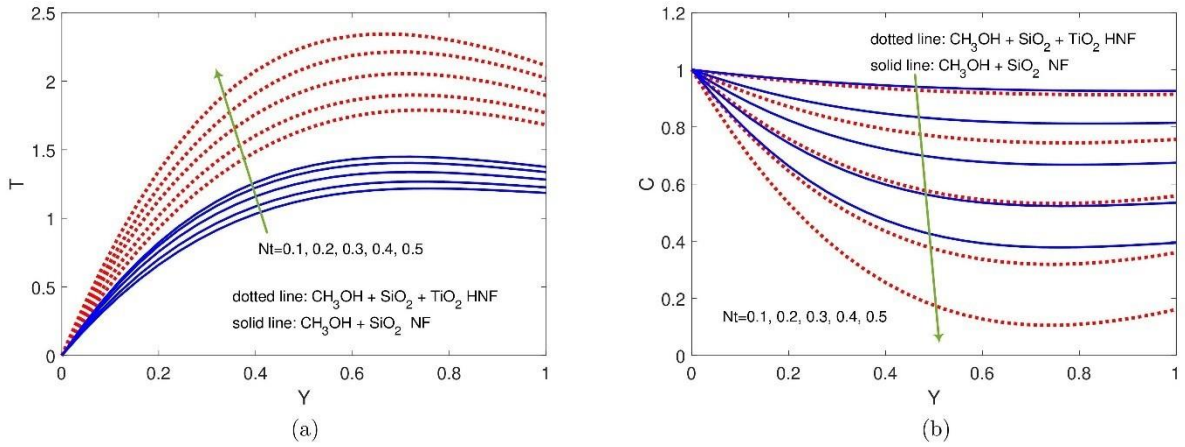

Figure 6: Impression of Nt on (a) velocity (b) temperature (c) concentration for =0.05, M=1, Kr=0.1, Ec=1, Pr=6.83, Bi=1, Nb=0.4, Le=1.

Figure 6 portrays the profiles of temperature and nanoparticle concentration for the variation of thermophoresis parameter(Nt). The upsurge in thermophoresis elevates the temperature and deteriorates the concentration in the channel. The temperature profile is observed to be higher for SiO2-TiO2-CH3OH HNF than that of SiO2 -CH3OH NF. The concentration profile is observed to be lower for of SiO2-TiO2-CH3OH HNF than that of SiO2 -CH3OH NF.

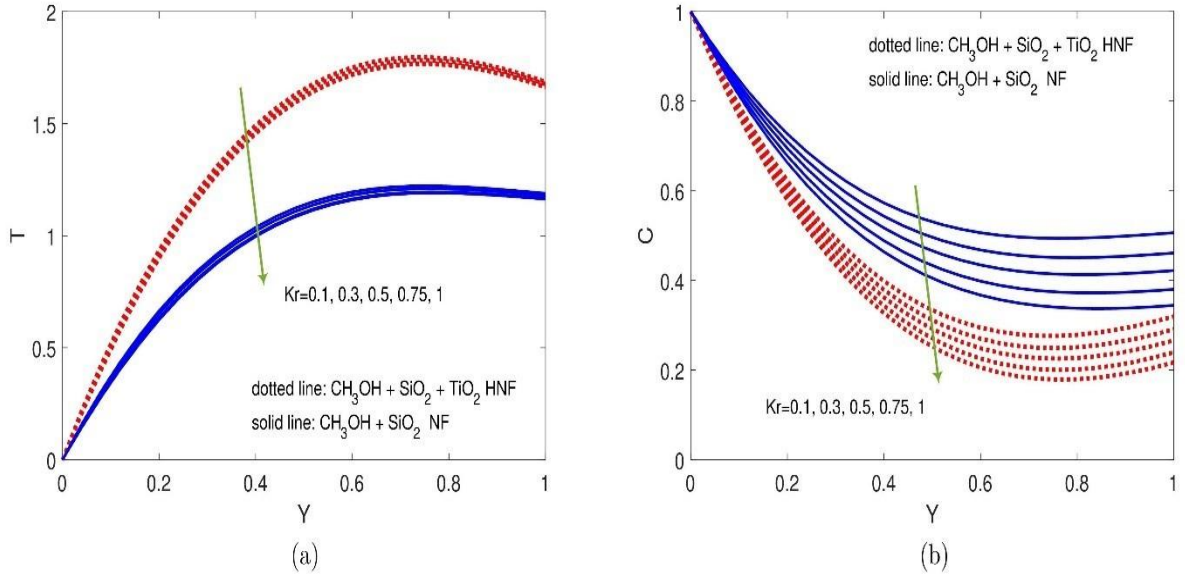

Figure 7: Impression of Nt on (a) velocity (b) temperature (c) concentration for =0.05, M=1, Kr=0.1, Ec=1, Pr=6.83, Bi=1, Nb=0.4, Le=1.

Figure 7 describes the profiles of temperature and nanoparticle concentration for the variation of chemical reaction parameter(Kr). The upsurge in Kr elevates the temperature and deteriorates the concentration in the channel. The temperature profile is observed to be higher for SiO2-TiO2-CH3OH HNF than that of SiO2 -CH3OH NF. The concentration profile is observed to be lower for of SiO2-TiO2-CH3OH HNF than that of SiO2 -CH3OH NF.

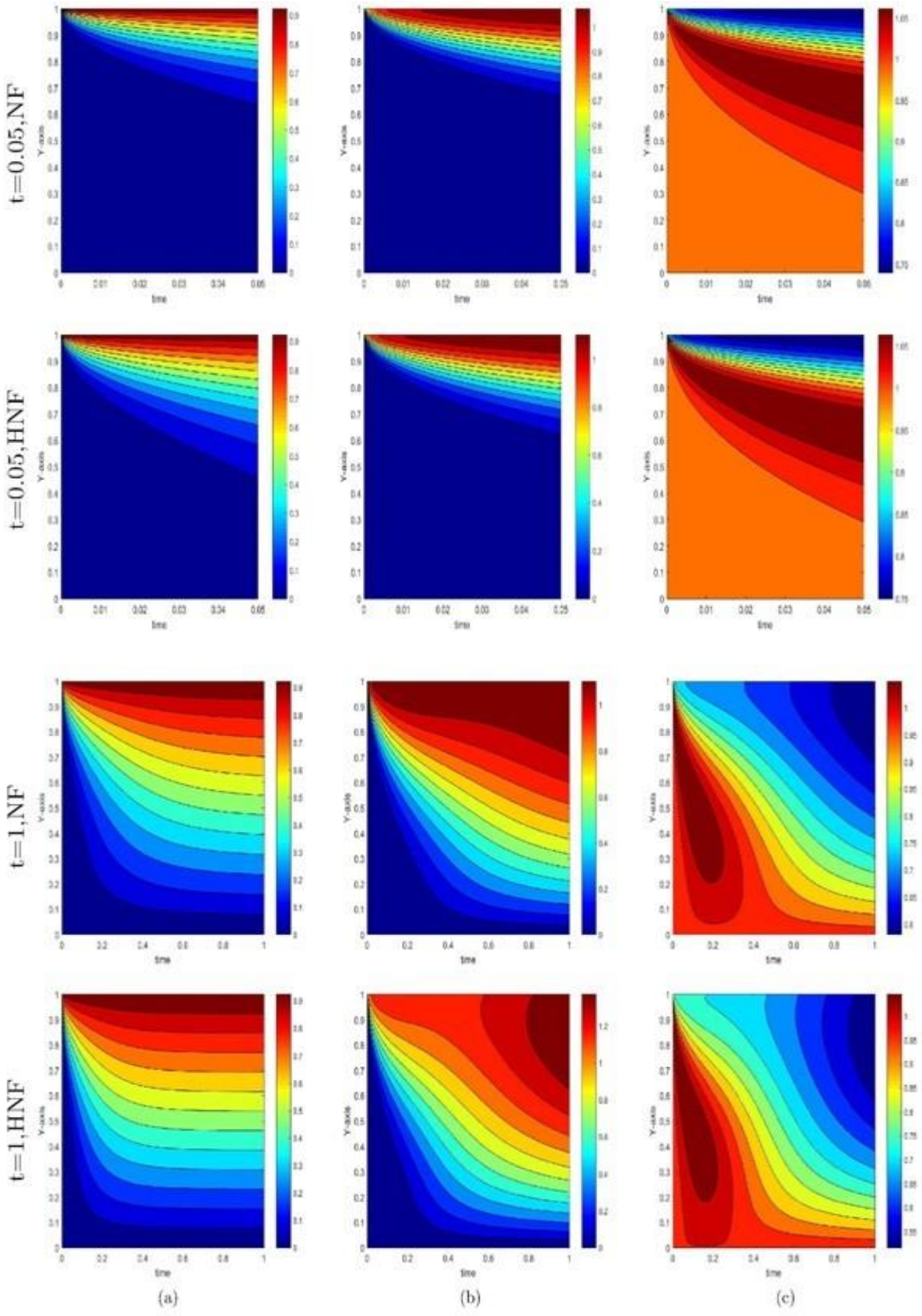

Figure 8: Contours of (a) velocity (b) temperature (c) concentration for diverse values of time and NF, HNF.

Figure 8 displays contours of velocity, temperature and concentration for the variation of time and NF, HNF. From figure 8(a) it is detected that the velocity boundary layer grows when the SiO2-CH3OH NF is changed to SiO2-TiO2-CH3OH HNF for the time t=0.05. As the time advances to t=1, the boundary layer improves near the lower plate. Figure 8(b) reveals that, the temperature near the hot wall gradually transfer to bottom wall. The temperature boundary layer thickness enhances when NF is changed to HNF for t=0.05. As the time advances to t=1, the boundary layer thickness of temperature is maximised. Maximum temperature cell is observed for . From figure 8(c) it is observed that the boundary layer of concentration is distributed from lower wall to upper wall. The concentration is maximum for , when t=0.05. As the time progresses to t=0.4, the cell maximum concentration is spread to . Maximum concentration is observed for when the time t=0.1.

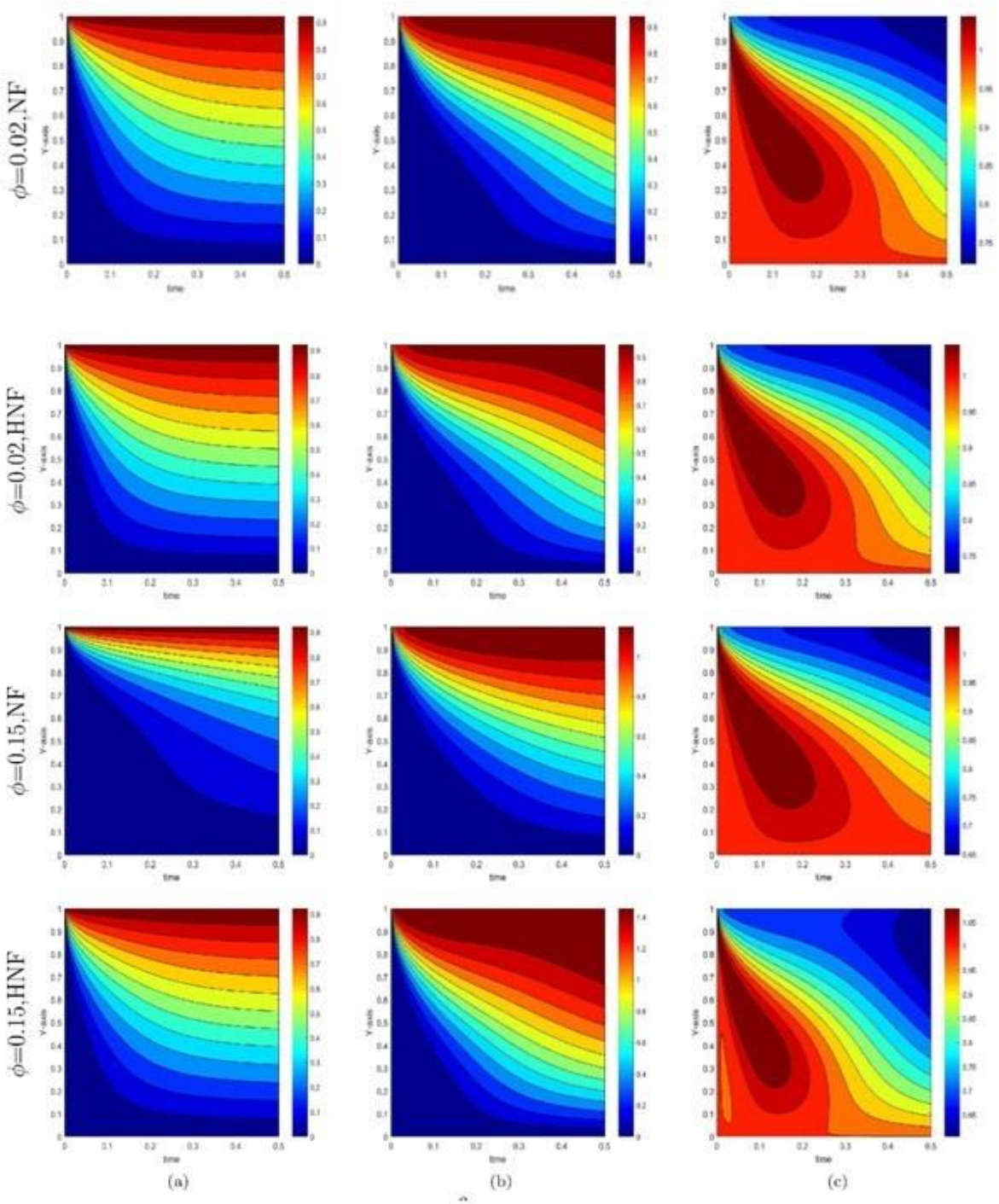

Figure 9: Contours of (a) velocity (b) temperature (c) concentration for diverse values of nanoparticle volume fraction and NF, HNF.

Figure 9 displays contours of velocity, temperature and concentration for the variation of nanoparticle volume fraction and NF, HNF at time t=0.5. From figure 9(a) it is observed that the velocity profile gradually declines from upper wall to lower wall for SiO2-CH3OH NF and SiO2-TiO2-CH3OH HNF. As the NVF increases to , velocity gradient is observed at hot wall. Figure 9(b) reveals that, the temperature profile gradually decreases from upper wall to lower wall for SiO2-CH3OH NF and SiO2-TiO2-CH3OH HNF. As the nanoparticle volume fraction increases to , the maximum temperature is observed in the range for SiO2-CH3OH NF. This range grows to for SiO2-TiO2-

CH3OH HNF. From figure 9(c) it is detected that, the cell with maximum concentration is observed throughout the channel in for . This is spread to for . When NF in the channel is changed to HNF a diminution in the concentration boundary layer is observed.

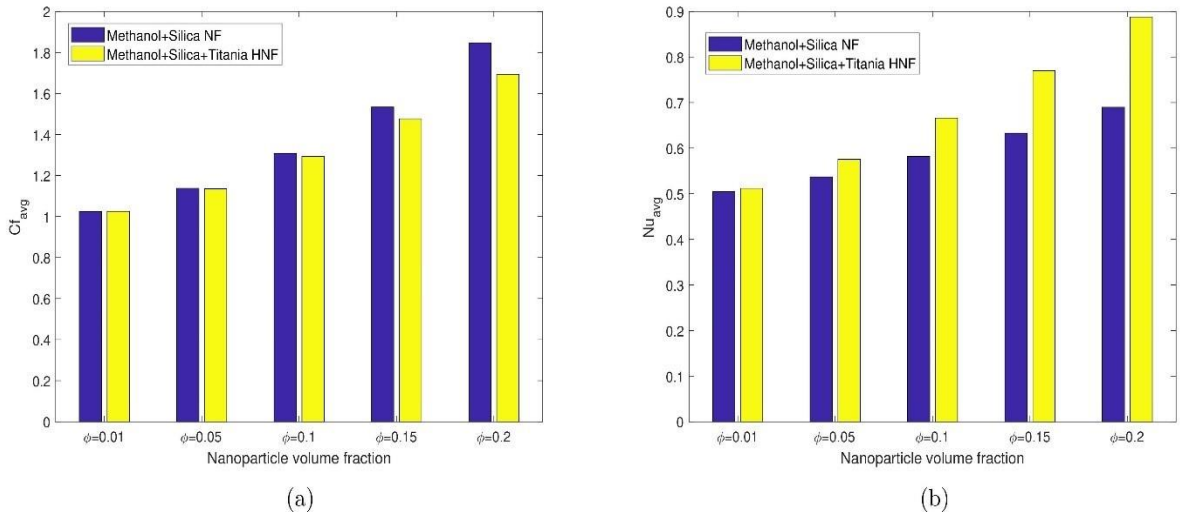

Figure 10: Impression of NVF on (a) skin friction coefficient (b) Nusselt number for NF, HNF.

Figure 10 displays the average coefficients of skin friction (Cf_{avg}) and Nusselt number (Nu_{avg}) for the variation of NF, HNF and NVF. When the NVF increases from $\phi = 0.01$ to $\phi = 0.2$, the Cf_{avg} and Nu_{avg} increases for SiO2-CH3OH NF and SiO2-TiO2-

CH3OH HNF. Interestingly, it is experiential that Nu_{avg} is higher for HNF and skin friction is higher for NF.

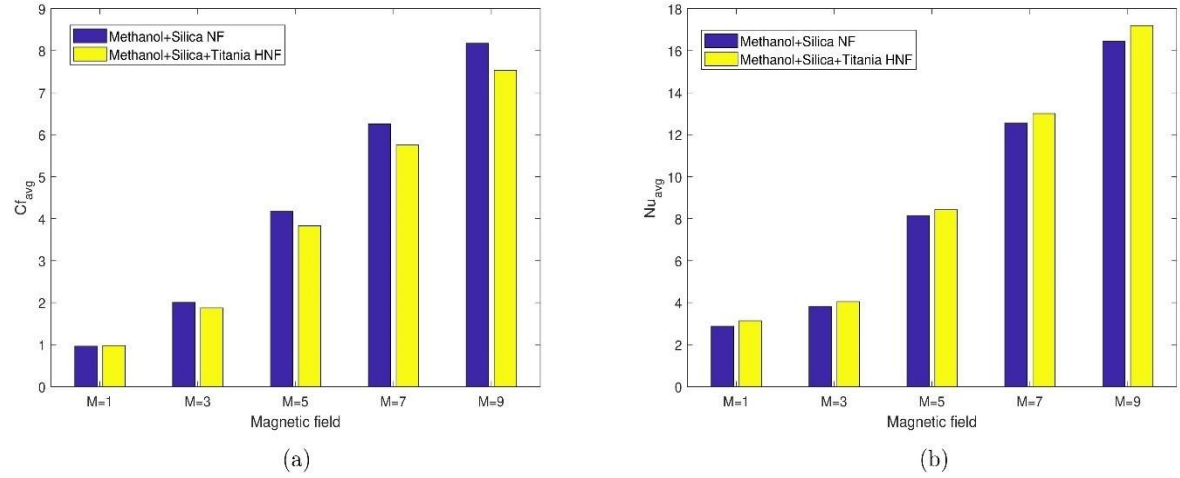

Figure 11: Impression of magneticfield on (a) skin friction coefficient (b) Nusselt number for NF, HNF.

Figure 11 displays Cf_{avg} and Nu_{avg} for the variation of NF, HNF and magnetic field. When the magnetic field increases from $M = 1$ to $M = 9$, the Cf_{avg} and Nu_{avg} increases for SiO2CH3OH NF and SiO2-TiO2-CH3OH HNF. Interestingly, it is experiential that Nu_{avg} higher for HNF and skin friction is higher for NF.

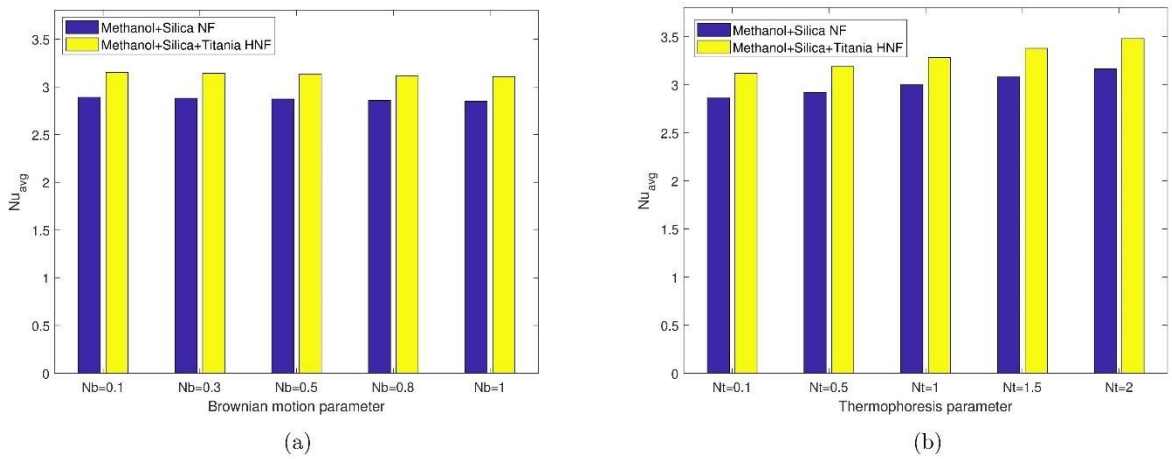

Figure 12: Impression of (a) Brownian motion (b) thermophoretic force on Nusselt number for NF, HNF.

Figure 12(a) displays Nu_{avg} for the variation of NF, HNF and Brownian motion. When the

Brownian motion parameter increases from $Nb = 0.1$ to $Nb = 1$, average Nusselt number decreases slightly for NF and HNF. Figure 12(b) displays the average Nusselt number for the variation of NF, HNF and Brownian motion. When the Brownian motion parameter increases from $Nt = 0.1$ to $Nt = 2$, average Nusselt number increases slightly for NF and HNF. The is higher for HNF.

Table 3: Skin friction coefficient for diverse values of t, M and ϕ.

			Lower plate y=0		**Upper plate y=1**	
Time	**phi**	**M**	**NF**	**HNF**	**NF**	**HNF**
0.1	0.02	1	0.7832	0.7837	1.7154	1.6447
0.1	0.02	2	0.5292	0.5288	2.8904	2.7039
0.1	0.02	3	0.3314	0.3302	5.0633	4.6633
0.1	0.05	1	0.8084	0.8075	2.0229	1.8059
0.1	0.08	1	0.8458	0.8385	2.3904	1.9708
0.5	0.02	1	1.4847	1.4538	0.4530	0.5109
0.5	0.02	2	0.7497	0.7620	1.8287	1.7380
0.5	0.02	3	0.3592	0.3646	4.4936	4.1249
0.5	0.05	1	1.6221	1.5408	0.4518	0.6015
0.5	0.08	1	1.7725	1.6359	0.4535	0.6991
8	0.02	1	1.5027	1.4668	0.4231	0.4905
8	0.02	2	0.7522	0.7642	1.8175	1.7296
8	0.02	3	0.3592	0.3647	4.4933	4.1245
8	0.05	1	1.6554	1.5555	0.3946	0.5790

8	0.08	1	1.8299	1.6520	0.3502	0.6754

Table 4: Nusselt number for diverse values of t, ϕ , M, Ec, Nb, Nt, Kr and Le at lower plate and upper plate.

								Lower plate y=0		**Upper plate y=1**	
Time	**phi**	**M**	**Ec**	**Nb**	**Nt**	**Kr**	**Le**	**NF**	**HNF**	**NF**	**HNF**
0.1	0.02	1	1	0.4	0.2	0.1	1	0.1870	0.2107	0.2264	0.1991
0.1	0.02	2	1	0.4	0.2	0.1	1	0.1018	0.1131	-0.0010	-0.0259
0.1	0.02	3	1	0.4	0.2	0.1	1	0.0499	0.0544	-0.4579	-0.4775
0.1	0.05	1	1	0.4	0.2	0.1	1	0.1577	0.2134	0.2372	0.1629
0.1	0.08	1	1	0.4	0.2	0.1	1	0.1354	0.2204	0.2513	0.1221
0.5	0.02	1	1	0.4	0.2	0.1	1	2.7845	3.0175	0.2679	0.2274
0.5	0.02	2	1	0.4	0.2	0.1	1	1.3643	1.5453	-0.1997	-0.2439
0.5	0.02	3	1	0.4	0.2	0.1	1	0.8474	0.9436	-1.4197	-1.4550
0.5	0.05	1	1	0.4	0.2	0.1	1	2.6939	3.3172	0.2963	0.1884
0.5	0.08	1	1	0.4	0.2	0.1	1	2.5953	3.6613	0.3263	0.1420
8	0.02	1	1	0.4	0.2	0.1	1	5.6630	6.0936	-0.5940	-0.7273
8	0.02	2	1	0.4	0.2	0.1	1	4.6426	5.0817	-1.4758	-1.6249
8	0.02	3	1	0.4	0.2	0.1	1	6.3913	6.7275	-4.0061	-4.1368
8	0.05	1	1	0.4	0.2	0.1	1	5.4001	6.4912	-0.4692	-0.8064
8	0.08	1	1	0.4	0.2	0.1	1	5.1552	6.9281	-0.3495	-0.8959
8	0.02	1	0.1	0.4	0.2	0.1	1	1.0297	1.0763	0.4162	0.4069
8	0.02	1	0.5	0.4	0.2	0.1	1	3.0848	3.3012	-0.0324	-0.0967
8	0.02	1	1	0.8	0.2	0.1	1	5.6212	6.0481	-0.5897	-0.7227
8	0.02	1	1	1.5	0.2	0.1	1	5.5487	5.9694	-0.5823	-0.7145
8	0.02	1	1	0.4	0.8	0.1	1	5.7615	6.2093	-0.6053	-0.7407
8	0.02	1	1	0.4	1.5	0.1	1	5.8799	6.3486	-0.6186	-0.7564
8	0.02	1	1	0.4	0.2	0.4	1	5.6324	6.0673	-0.5912	-0.7250
8	0.02	1	1	0.4	0.2	0.7	1	5.6067	6.0450	-0.5890	-0.7232
8	0.02	1	1	0.4	0.2	0.1	3	5.6501	6.0850	-0.5942	-0.7283
8	0.02	1	1	0.4	0.2	0.1	6	5.6536	6.0973	-0.5975	-0.7329

5. Conclusions

This article inspects the impacts of methanol-silica-titania HNF and methanol-silica NF associated with chemical reaction on the Couette flow in a channel. The calculation of outcomes is accomplished by functioning the FDM. The deductions are detailed as come after:

- The velocity profile is diminished with magnetic field(M) and nanoparticle volume fraction(ϕ).

- The temperature profile is boosted with magnetic field(M), Eckert number(Ec), thermophoresis(Nt) and nanoparticle volume fraction(ϕ). In contrast, Brownian motion(Nb) reduced the temperature profile.

- The nanoparticle concentration profile is deteriorated with magnetic field(M), Eckert number(Ec), thermophoresis(Nt) and nanoparticle volume fraction(ϕ). In contrast, Brownian motion(Nb) elevated the concentration profile.

- Further, the velocity and temperature contours located with maximum magnitude near upper plate, while concentration contours located with higher magnitude throughout the channel. As the time progresses beyond t=0.3, the higher concentration is present near lower plate. HNF increases the boundary layer thicknesses of velocity and temperature.

- Cf_{avg} and Nu_{avg} increased with magnetic field and nanoparticle volume fraction. Nu_{avg} is increased with thermophoresis parameter. Hybrid nanofluid shows higher

performance compared to nanofluid in case of average Nusselt number.

REFERENCES

1. Choi, S.U.S.; Eastman, J.A. Enhancing Thermal Conductivity of Fluids with Nanoparticles: Technical Report ANL/MSD/CP-84938; CONF-951135-29; Argonne National Lab.: Lemont, IL, USA, 1995.
2. Choi, S. Enhancing thermal conductivit of fluids with nanoparticles. In Developments and Applications of Non-Newtonian Flows; Siginer, D.A.,Wang, H.P., Eds.; FEDV.231/MD-V; ASME: New York, NY, USA, 1995; Volume 66, pp. 99–105.
3. Panduro, E.A.C.; Finotti, F.; Largiller, G.; Lervåg, K.Y. A review of the use of nanofluids as heat-transfer fluids in parabolic-trough collectors. Appl. Therm. Eng. 2022, 211, 118346.
4. Yan, S.R.; Aghakhani, S.; Karimipour, A. Influence of a membrane on nanofluid heat transfer and irreversibilities inside a cavity with two constant-temperature semicircular sources on the lower wall: Applicable to solar collectors. Phys. Scr. 2020, 95, 085702.
5. Sheremet, M.A.; Pop, I.; Mahian, O. Natural convection in an inclined cavity with time-periodic temperature boundary conditions using nanofluids: Application in solar collectors. Int. J. Heat Mass Transf. 2018, 116, 751–761.
6. Tiwari RK, Das MK. Heat transfer augmentation in a two-sided lid-driven differentially heated square cavity utilizing nanofluids. International Journal of heat and Mass transfer. 2007;50(9-10):2002-18.
7. N. Biswas, N. K. Manna, P. Datta, and P. S. Mahapatra, "Analysis of heat transfer and pumping power for bottom-heated porous cavity saturated with Cu-water nanofluid," Powder Technol. 326, 356–369 (2018).
8. K. Khanafer and K. Vafai, "Applications of nanofluids in porous medium," J. Therm. Anal. Calorim. 135, 1479–1492 (2019).
9. Saha G, Paul MC. Investigation of the characteristics of nanofluids flow and heat transfer in a pipe using a single phase model. International Communications in Heat and Mass Transfer. 2018;93:48-59.
10. Manca O, Nardini S, Ricci D. A numerical study of nanofluid forced convection in ribbed channels. Applied Thermal Engineering. 2012 May 1;37:280-92.
11. Ahmed MA, Yaseen MM, Yusoff MZ. Numerical study of convective heat transfer from tube bank in cross flow using nanofluid. Case studies in thermal engineering. 2017;10:560-9.
12. Vajjha RS, Das DK, Namburu PK. Numerical study of fluid dynamic and heat transfer performance of Al2O3 and CuO nanofluids in the flat tubes of a radiator. International Journal of Heat and fluid flow. 2010;31(4):613-21.
13. J. Buongiorno, Convective Transport in Nanofluids, J. Heat Transfer. 128 (2006) 240. doi:10.1115/1.2150834
14. M. Mahmoodi, S. Kandelousi, Effects of thermophoresis and Brownian motion on nanofluid heat transfer and entropy generation, J. Mol. Liq. 211 (2015) 15–24. doi:10.1016/j.molliq.2015.06.057
15. S.Y. Motlagh, H. Soltanipour, Natural convection of Al2O3-water nanofluid in an inclined cavity using Buongiorno's two-phase model, Int. J. Therm. Sci. 111 (2017) 310–320. doi:10.1016/j.ijthermalsci.2016.08.022.
16. M.A. Sheremet, I. Pop, Free convection in a porous horizontal cylindrical annulus with a nanofluid using Buongiorno's model, Comput. Fluids. 118 (2015) 182–190. doi:10.1016/j.compfluid.2015.06.022.
17. M.A. Sheremet, I. Pop, M.M. Rahman, Three-dimensional natural convection in a porous enclosure filled with a nanofluid using Buongiorno's mathematical model,
18. Int. J. Heat Mass Transf. 82 (2015) 396–405. doi:10.1016/j.ijheatmasstransfer.2014.11.066.
19. R. Subba, R. Gorla, B. Vasu, S. Siddiqa, Transient Combined Convective Heat Transfer over a Stretching Surface in a Non-Newtonian Nanofluid Using Buongiorno ' s Model, J. Appl. Math. Phys. 4 (2016) 443–460. doi:10.1166/jon.2016.1242.
20. Ali, A. O., & Makinde, O. D. (2015). Modelling the Effect of Variable Viscosity on Unsteady Couette Flow of Nanofluids with Convective Cooling. Journal of Applied Fluid Mechanics, 8(4). 793-802.
21. Tlili, I., Hamadneh, N.N., Khan, W.A. et al. Thermodynamic analysis of MHD Couette–Poiseuille flow of water-based nanofluids in a rotating channel with radiation and Hall effects. J Therm Anal Calorim 132, 1899–1912 (2018).
22. Hajmohammadi, M. R. (2017). Cylindrical Couette flow and heat transfer properties of nanofluids; single-phase and two-phase analyses. Journal of Molecular Liquids, 240, 45-55.
23. Karim, M. E., Samad, M. A., & Ferdows, M. (2019, July). Numerical study of the effect of variable viscosity on unsteady pulsatile nanofluid flow through a Couette channel of stretching wall with convective heat transfer. In AIP Conference Proceedings (Vol. 2121, No. 1, p. 070005). AIP Publishing LLC.
24. G. Huminic and A. Huminic, "Hybrid nanofluids for heat transfer applications—A state-of-the-art review," Int. J. Heat Mass Transfer 125, 82–103 (2018).
25. H. M. Ali, Hybrid Nanofluids for Convection Heat Transfer, Academic Press, London, UK, 2020.
26. N. A. C. Sidik, I. M. Adamu, M. M. Jamil, G. H. R. Kefayati, R. Mamat, and G. Najafi, "Recent progress on hybrid nanofluids in heat transfer applications: A comprehensive review," Int. Commun. Heat Mass Transfer 78, 68–79 (2016).
27. Hayat T, Nadeem S. Heat transfer enhancement with Ag–CuO/ water hybrid nanofluid. Results Phys. 2017;7:2317–24.

28. Ghadikolaei SS, Hosseinzadeh K, Ganji DD. Investigation on ethylene glycol-water mixture fluid suspend by hybrid nanoparticles (TiO2–CuO) over rotating cone with considering nanoparticles shape factor. J Mol Liq. 2018;272:226–36. https ://doi. org/10.1016/j.molli q.2018.09.084.
29. Waini I, Ishak A, Pop I. Hybrid nanofluid flow and heat transfer over a nonlinear permeable stretching/shrinking surface. Int J Numer Methods Heat Fluid Flow. 2019; 29: 3110–27. https ://doi. org/10.1108/HFF-01-2019-0057.
30. Bagheri H, Behrang M, Assareh E, Izadi M, Sheremet MA. Free convection of hybrid nanofluids in a C-shaped chamber under variable heat flux and magnetic field: simulation, sensitivity analysis, and artificial neural networks. Energies. 2019;12:1–
31. 17. https ://doi.org/10.3390/en12142807 .
32. Ali Lunda L, Omara Z, Khan I, Seikh A, El-Sayed H, Sherif M, Nisar KS. Stability analysis and multiple solution of Cu–Al2O3/ H2O nanofluid contains hybrid nanomaterials over a shrinking surface in the presence of viscous dissipation. J Matter Res Technol. 2020;9(1):421–32.
33. Swain K, Mebarek-Oudina F, Abo-Dahab SM. Influence of MWCNT/Fe3O4 hybrid nanoparticles on an exponentially porous shrinking sheet with chemical reaction and slip boundary conditions. Journal of Thermal Analysis and Calorimetry. 2022 Jan;147(2):1561-70.
34. Sheikholeslami M, Ganji DD, Rashidi MM. Magnetic field effect on unsteady nanofluid flow and heat transfer using Buongiorno model. Journal of Magnetism and Magnetic Materials. 2016 Oct 15;416:164-73.
35. Ghalambaz M, Doostani A, Izadpanahi E, Chamkha AJ. Conjugate natural convection flow of Ag–MgO/water hybrid nanofluid in a square cavity. Journal of Thermal Analysis and Calorimetry. 2020 Feb;139(3):2321-36.
36. Xuan Y, Duan H, Li Q. Enhancement of solar energy absorption using a plasmonic nanofluid based on TiO2/Ag composite nanoparticles. RSC Adv. 2014;4(31):16206–13.
37. Madhesh D, Parameshwaran R, Kalaiselvam S. Experimental investigation on convective heat transfer and rheological characteristics of Cu–TiO2 hybrid nanofluids. Exp Thermal Fluid Sci. 2014;52:104–15.
38. Sundar LS, Singh MK, Sousa AC. Enhanced heat transfer and friction factor of
39. MWCNT–Fe3O4/water hybrid nanofluids. Int Commun Heat Mass Transf. 2014;52:73–83.
40. Sarkar J, Ghosh P, Adil A. A review on hybrid nanofluids: recent research, development and applications. Renew Sustain Energy Rev. 2015;43:164–77.
41. Chen Z, Arce P. An integral-spectral approach for convective-diffusive mass transfer with chemical reaction in Couette flow Mathematical formulation and numerical illustrations. Chemical Engineering Journal. 1997; 68(1):11-27.
42. Abbaszadeh M, Bayat M, Dehghan M, Azis MI. Investigation of generalized Couette hydromagnetic flow of two-step exothermic chemical reaction in a channel via the direct meshless local Petrov–Galerkin method. Engineering Analysis with Boundary Elements. 2021;125:178-89.
43. Kareem RA, Gbadeyan JA. Entropy generation and thermal criticality of generalized Couette hydromagnetic flow of two-step exothermic chemical reaction in a channel. International Journal of Thermofluids. 2020;5:100037.
44. Ahmad, S., Kalita, D.: Laplace technique on magnetohydrodynamic radiating and chemically reacting fluid over an infinite vertical surface. Int. J. Sci. Technol. 1, 224– 233 (2012)
45. Muthucumaraswamy, R., Ganesan, P.: Effect of the chemical reaction and injection on flow characteristics in an unsteady upward motion of an isothermal plate. J. Appl. Mech. Tech. Phys. 42, 665–671 (2001)
46. Dulal, P., Babulal, T.: Combined effects of Joule heating and chemical reaction on unsteady magnetohydrodynamic mixed convection of a viscous dissipating fluid over a vertical plate in porous media with thermal radiation. Math. Comput. Model. 54, 3016–3036 (2011)
47. Patil, P.M., Kulkarmi, P.S.: Effects of chemical reaction on free convective flow for a polar fluid through a porous medium in the presence of internal heat generation. Int. J. Thermal Sci. 47, 1043–1054 (2008)
48. Kesavaiah, D.C., Satyanarayana, P.V., Venkataramana, S.: Radiation absorption, chemical reaction and magnetic field effects on the free convection and mass transfer flow through porous medium with constant heat flux. Int. J. Sci. Eng. Technol. 1, 274–284 (2012)
49. Ibrahim, F.S., Elaiw, A.M., Bakr, A.A.: Effect of chemical reaction and radiation absorption on the unsteadyMHD free convection flow past a semi infinite vertical permeable moving plate with heat source and suction. Commun. Nonlinear Sci. Numer. Simul. 13, 1056–1066 (2008)